Ephedrine sensing at the electrified liquid-liquid interface supported with micro-punched self-adhesive polyimide film

Paulina Borgul, Patrycja Pawlak, Konrad Rudnicki, Karolina Sipa, Pawel Krzyczmonik, Anna Trynda, Slawomira Skrzypek, Grégoire Herzog, Lukasz Poltorak

Sensors & Actuators: B. Chemical 344 (2021) 130286

Contents lists available at ScienceDirect

Sensors and Actuators: B. Chemical

journal homepage: www.elsevier.com/locate/snb

Ephedrine sensing at the electrified liquid-liquid interface supported with micro-punched self-adhesive polyimide film

Paulina Borgul [a], Patrycja Pawlak [a], Konrad Rudnicki [a], Karolina Sipa [a], Pawel Krzyczmonik [a], Anna Trynda [b], Slawomira Skrzypek [a], Grégoire Herzog [c], Lukasz Poltorak [a,*]

[a] Department of Inorganic and Analytical Chemistry, Electroanalysis and Electrochemistry Group, Faculty of Chemistry, University of Lodz, Tamka 12, 91-403, Lodz, Poland
[b] Chemistry Department, Central Forensic Laboratory of the Police, Warsaw, Poland
[c] Université de Lorraine, CNRS, LCPME, F-54000, Nancy, France

ARTICLE INFO

Keywords:
ITIES
Ion transfer voltammetry
Illicit drugs precursor
Miniaturization
Ephedrine sensor
Caffeine

ABSTRACT

In this work, ephedrine was studied at the electrified liquid-liquid interface (LLI) supported with an array of apertures micro-punched in the self-adhesive polyimide tape. During LLI miniaturization protocol development, we have tested three arrays of needles (each containing 12, 24, or 36 pre-arranged units) used to puncture the polyimide film. Since all needles have a conical shape at the sharp site end we have created and tested the membranes with controlled penetration depth allowing for the adjustment of the pores dimensionality. The resulting membranes were characterized with ion transfer voltammetry and scanning electron microscopy. The best results were obtained for 12 micro-punched pores made with the highest studied penetration depth (equal to 1450 μm), and hence, this configuration was employed for the ephedrine sensing. As the electroanalytical method, we have employed ion transfer voltammetry (ITV). The miniaturization allowed for the ephedrine detection down to 1 μM. Ephedrine was measured alone and in the presence of caffeine.

1. Introduction

Intriguing charge transfer processes happening at the interface between two immiscible liquids, although still not fully understood, are used for a variety of applications. When a proper experimental configuration is assured (including both immiscible solvents, electrolytes, and hardware connections) one can directly record currents originating from the ions or electrons crossing this soft, polarizable junction. This phenomenon was significantly developed by Koryta in the 70 s [1], and still, after more than 50 years, scientists debate about its fundamental nature [2,3]. The interface between two immiscible electrolyte solutions (ITIES) is usually formed between the aqueous electrolyte solution of highly hydrophilic salt (e.g. sodium chloride) and the organic solution of highly hydrophobic salt dissolved in an appropriate organic solvent [4]. Formed liquid-liquid interface (LLI) can be polarized and used to study interfacial charge transfer processes such as electron transfer reaction, ion transfer reaction, facilitated ion transfer reaction, or coupled electron and ion transfer reactions [2,5]. These processes can be applied in many fields (still limited to fundamental studies) such as ionic extraction [6,7], LLI modification with smart materials [8,9], drug delivery and release studies [10], biological membrane mimicking platforms [10,11] and finally chemical detection [12–15].

ITIES miniaturization attracted significant attention over the last few decades as it brings additional benefits (especially) to electroanalytical studies. (i) Enhancement of a mass transfer through the ordering of the diffusion field(s) to the shape of a hemisphere(s) improves sensing sensitivity whereas, (ii) lower values of capacitive currents further improving the lower detection limits [16]. (iii) Additionally, miniaturization adds to the stability of the electrified LLI and even allows for (iv) the measurements in the media with uncompensated iR drop (e.g. with the organic phase deprived of the background electrolyte). In a view of electroanalytical applications, the electrified LLI miniaturization may also lead to undesired effects such as interface movement influencing its location within the support [17,18], that may appear especially when sufficiently low (or high) potential difference is applied to a biphasic system. Micro- or nano-ITIES were applied in many analytical studies including street drug samples [19], refined drug distribution [20,21], vitamins [22], insecticide agents [23], analysis of body fluids [24,25],

* Corresponding author.
E-mail address: lukasz.poltorak@chemia.uni.lodz.pl (L. Poltorak).

https://doi.org/10.1016/j.snb.2021.130286
Received 7 April 2021; Received in revised form 3 June 2021; Accepted 9 June 2021
Available online 11 June 2021

pathogenic bacteria biomarkers [26], environmental contaminants [27] among many other. The crucial aspect of ITIES miniaturization relies on the preparation of support equipped with a single/array of nano/micro-pores. A few miniaturization protocols burdened with different preparation difficulties exist to date. Taylor and Girault used a glass tube that upon heating and pulling formed a micro-aperture that was further used to support ITIES [28]. The same team also developed a miniaturization protocol based on a thin polymer sheet with a single micro-hole made using laser ablation [29]. Another method proposed in the literature for creating microITIES was to enclose the micro-wire in the glass capillary, followed by its dissolution, and finally the formation of a micro-cavity [30]. Single micro-pore can be also formed using simple processing involving heat shrinkable tubes and fused silica capillaries [31]. Faisal et al. developed a method where thin PVC film (12 μm thick) was punctured with the shar needle leaving a single ellipse shaped micro aperture [32]. The advancement of technology in the last few years has allowed for further improvement and extensions of microITIES [31,33], as well as nanoITIES fabrication procedures [34–36]. However, in the majority of cases, these protocols rely on advanced and/or costly instrumentation which limits the accessibility, and hence application and development, of the LLI miniaturized supports. We wish to tackle this problem, by proposing simple miniaturization solutions that can be performed with the widely accessible tools and materials.

The array of microITIES developed in this work is used as a platform for ephedrine determination alone and in the presence of caffeine. Ephedrine is a natural alkaloid, commercially extracted from the Ephedra plants. This compound is commonly used as a medication, stimulant, and also as a precursor for illicit drug(s) synthesis [37,38]. Due to its structural similarity, ephedrine is used as a precursor for the production of amphetamine and methamphetamine (the consumption of these two drugs in Europe is still increasing) [39]. Not many studies have assessed the toxicity of ephedrine. Nevertheless, its lethal dose for humans is estimated to be around 50 mg kg^{-1} [40]. Among athletes, ephedrine is prohibited when it is present in the urine at a concentration of 10 mg ml^{-1} or higher [38]. The supplements being a mixture of ephedrine and caffeine are very popular formulations used for weight loss [41] (*e.g.* it was shown that a mixture of caffeine and ephedrine (200 mg and 20 mg, respectively) is more effective in losing weight than these chemical species taken alone [42,43]. Especially due to applications in illicit drug synthesis, ephedrine production, and handling have to be closely monitored. This is a difficult task because ephedrine is an ingredient in dozens of over-the-counter medications from which it can be easily extracted. Some EU countries imposed additional control over medicines containing ephedrine, but this has not fully resolved the problem due to easy access in other countries [44]. All these indicate, that simple sensing protocols for ephedrine detection should be in high demand.

In our work, microITIES has been prepared using a very simple, do-it-yourself (DIY) microfabrication protocol. The entire processing requires readily available and very cheap materials. It has to be underlined that no sophisticated instrumentation is needed to achieve repeatable and reproducible results. Developed platforms are based on the self-adhesive polyimide films micro-punched with an array of needles. The resulting micro-pattered membranes served as the ITIES support. As for the practical application, we have employed our system for ephedrine detection. The effect of caffeine interference was also investigated.

2. Methods and materials

2.1. Methods

The aqueous phase was 10 mM sodium chloride (NaCl, ChemPur, M =58.44 g mol^{-1}) dissolved in water distilled in triplicate. The organic phase background electrolyte was bis(triphenylphosphoranylidene) ammonium tetrakis(4-chlorophenyl)borate (BTPPATPBCl) synthesized by a simple metathesis reaction. Potassium tetrakis(4-chlorophenyl) borate (KTPBCl, 98 %, Sigma-Aldrich, M = 496.11 g mol^{-1}) and bis-(triphenylphosphoranylidene)ammonium chloride (BTPPACl, 97 %, Sigma-Aldrich M =574.03 g mol^{-1}) were used as the reaction substrates. BTPPATPBCl was dissolved in 1,2-dichloroethane (1,2-DCE, POCH, M =98.96 g mol^{-1}) that was further used as the organic phase. Interfacially active chemical species: tetramethylammonium chloride (TMACl, >98 %, Acros Organics, M =109.6 g mol^{-1}), ephedrine hydrochloride (>99 %, Sigma, M = 201.69 g mol^{-1}), caffeine (98.5 %, Acros Organics, M =194.19 g mol^{-1}) were always initially dissolved in the aqueous phase. After micro-puncturing, the self-adhesive polyimide tape (18 mm width, 0.05 mm thick) was attached to the glass tube (internal diameter = 6.0 mm, outer diameter = 9.0 mm, length = 55.0 mm) and was further secured on the edges with the silicone sealant (Diall, UK). Needle arrays and the device used to control the protrusion of the needle were manufactured by Glomeve, China (see Fig. SI2 for photos). The needles within array used to perform the analytical study had following dimensions. The thickness of the sharp end of the needle was equal to 10 μm (+/- 2 μm, n = 3), the thickness of needles measured 50 μm from the sharp point was equal to 35 μm (+/- 3 μm, n = 3), the thickness of needles measured 100 μm from the sharp point was equal to 50 μm (+/- 3 μm). Needle dimensions were measured using ImageJ software.

2.2. Electrochemical cell

All experiments described in this work were conducted in the electrochemical cell shown in Fig. SI1. In the presented system, three electrodes were used – two for the water phase and one for the organic phase. In the aqueous phase, the platinum wire was used as the counter electrode and Ag/AgCl wire was used as the reference electrode. In the organic phase, the silver wire served as the counter and the pseudo-reference electrode in one. Electrochemical measurements were performed using an Autolab 302 N equipped with EDC module.

Cell I shows the composition of the electrochemical cell used to study microITIES (eph – ephedrine; caf – caffeine):

$$Ag|AgCl|\begin{matrix}10\ mM\ NaCl\\ x\ mM\ TMA^{+}\ or\ eph\ or\ eph\ +\ caf\end{matrix}\Big|\Big|\begin{matrix}5\ mM\\ BTPPATPBCl\end{matrix}|Pt$$

2.3. Optical microscopy

Optical microscopy (MMT 800BT, mikroLAB, Lublin, Poland) was used to visualize punched micropores. We have prepared membranes containing 12, 24, and 36 micro-holes at all studied penetration depths (for 12 and 24 micro-needles 200, 700, 1200, and 1450 μm, for 36 micro-needles 50, 550, 1050, and 1300 μm). Shown images were taken at 5x magnification unless otherwise stated.

2.4. Scanning electron microscopy

Scanning electron microscopy (SEM) micrographs were obtained using a benchtop JCM-6000 (from JEOL, Japan). An acceleration voltage of 5 kV was used for imaging metallised polyimide membranes to avoid surface charging effects.

2.5. Miniaturization protocol

A simple self-adhesive polyimide tape-based miniaturization protocol (see Fig. 1) was developed to support LLI. The first fabrication step was to prepare a piece of the self-adhesive polyimide tape that was cut and then fixed to a spongy pad with the adhesive side facing upwards. The tape was used as received. No additional effort is needed to adjust tape chemical properties. We have used 18 mm wide, 50 μm thick polyimide tape produced by nicelux®. We assume that other similar tapes can be used instead. Next, an array of micro-holes was punctured in the

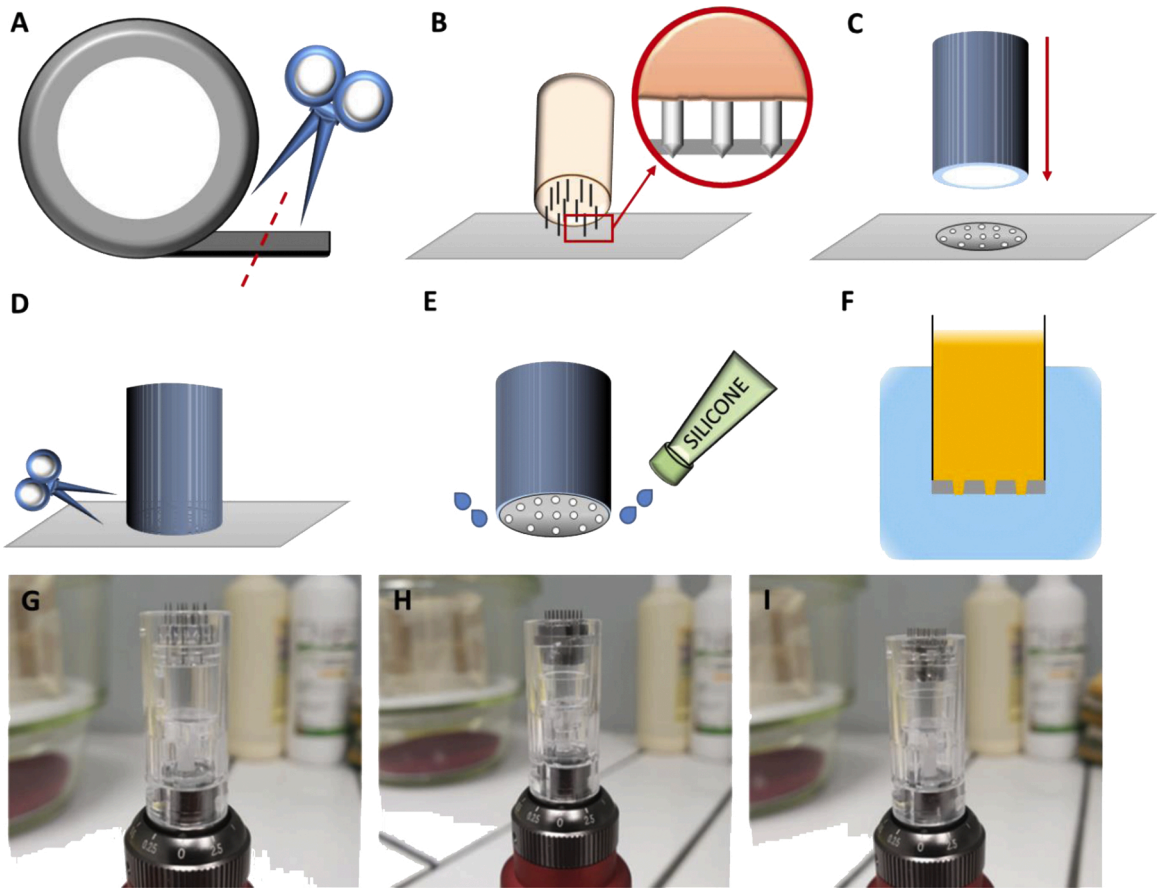

Fig. 1. Micro-punched polyimide film preparation protocol. A – cutting the section of the self-adhesive polyimide tape. B – puncturing polyimide tape with an array of micro-needles with a fixed penetration depth. C – fixing the punctured area to the glass tube (all pores should be located within the center of the tube opening). D – cutting out the circle defined by the glass tube walls. E – securing the glass membrane with a silicone sealant. F – filling the glass tube with the organic phase (orange color, upper phase) and immersing it into the aqueous phase (blue color, bottom phase). Photos of the needle arrays together with the base allowing for the protrusion control. G - 12 needles; H - 24 needles; I- 36 needles. (For interpretation of the references to colour in this figure legend, the reader is referred to the web version of this article).

tape (see Fig. 1B) using a commercially available head (derma cartridge by MyM®) equipped with pre-arranged micro-needles of fixed and adjustable length (see photos from Fig. 1G–I for details). The perforation was made by firmly and perpendicularly piercing the tape until the cartridge equipped with needles (protrusion was preset) was in direct contact with the adhesive side of the tape. The pad made out of a soft sponge hosted the sharp end of needles and prevented the needles from becoming blunt after the tape was punctured. Three arrays of needles each containing 12, 24, or 36 units were tested. The length of the needles was controlled with a screw within a pen (derma pen by MyM®, see Fig. 1G–I) giving the ability to define the protrusion, and hence, the penetration depth of a needle puncturing the tape and eventually going into the underlying pad. The reasoning behind adjusting the needle protrusion is related to the conical needle geometry. By varying the needle penetration depth we change the dimensionality of the pore at its entrance and exit. For heads with 12 and 24 needles, studied protrusions were equal to around 200 µm, 700 µm, 1200 µm, and 1450 µm. For the head with 36 needles in the array, the protrusions were equal to 50 µm, 550 µm, 1050 µm, and 1300 µm. The penetration depth equal to 50 µm for the array containing 36 was not enough to puncture the tape, and hence, this remained impenetrable. The penetration depth accuracy was calculated to be 50 µm. In the next step, a glass tube was attached to the punctured tape at the same time making sure that all pores are in the center of the tube opening (see Fig. 1C). The adhered membrane was cut along the glass tube walls (see Fig. 1D). Finally, to prevent any possible organic phase leakage, a small amount of silicone sealant was applied to a place where tape and glass tube meets. After the silicone glue solidified, the glass tube finished with a membrane was filled with the organic phase and was further placed in the electrochemical cell filled with the aqueous phase. The volume of the organic phase added to the glass tube and the position of the membrane from the Luggin capillary were kept constant during all experiments. Also, the membrane was always positioned only slightly below the surface of the aqueous phase. This arrangement prevented from an eventual leakage of the water phase to the glass tube filled with the organic phase. All membranes prepared in this way were tested in the cell I using interfacially active model ion – tetramethylammonium cation (TMA^+).

3. Results and discussion

3.1. Micropunched membranes characterization

The ITV was first used to investigate the effect of a number of micro-punctured pores within the created arrays and the needles penetration depth into the polyimide tape on the recorded ionic current intensities and voltammetric current-potential patterns. We have found that the resulting ITVs recorded in the presence of 40 µM TMA^+ crossing the interface supported with all prepared membranes (except for 36 needles extended at 50 µm which did not suffice to penetrate the polyimide tape) provided similar current – potential characteristics (Figs. 2A and SI 3A, B and C). On the forward polarization (from less to more positive potential values) the TMA^+ ions transfer from the aqueous to the organic phase

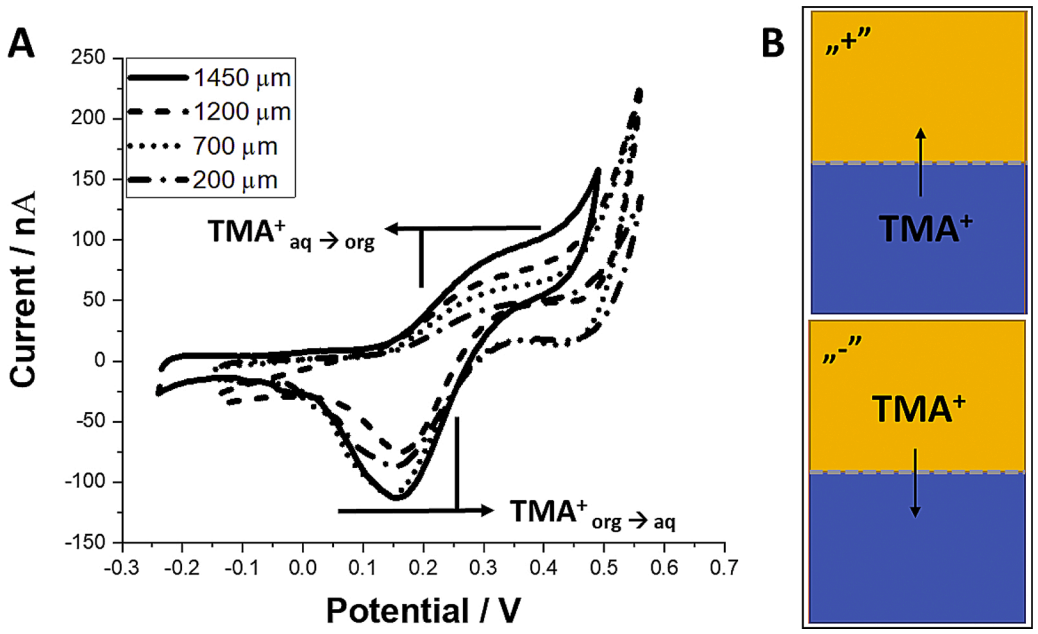

Fig. 2. A - ITVs recorded for [TMA^+] = 40 µM for four different penetration depths indicated in the figure legend punctured with the array of 12 needles (see section 3.1 for details). The scan rate was set to 25 mV·s^{-1}; B–C - scheme representing TMA^+ ion transport from the aqueous to the organic phase and from the organic to the aqueous phase. "+" and "-"signs in the upper left corner are given to indicate the sign of the recorded current.

giving a sigmoidal wave indicating a predominance of radial diffusion [31,33,45,46]. The back transfer happening within the organic phase, gave a negative signal having a shape of a peak with a diffusion-limited tail characteristic for a mass transfer limited by a linear diffusion. Fig. 3A shows the relationship between the recorded positive signal intensity ([TMA^+] = 40 µM) and the needles penetration depth for three investigated arrays (equipped with 12; 24 and 36 needle units). For all studied cases, the general dependency of increasing ionic current for the deeper puncture was observed and can be also directly visualized in Fig. 3A. This is an expected observation since all needles are conical in shape, and hence, their deeper protrusion leaves wider openings (see Fig. 3B and C). This is turn, is reflected as the increasing electrochemically active surface area of the ITIES formed within the pore.

The geometry of the sharp ends of the needles varies between arrays which have directly affected the final geometry and dimensionality of micro-punched openings within the membrane. Fig. 3B and C summarize the shorter (pore height) and longer (pore width) sections of the created openings. Needles from the array having 12 units gave the punctures with the most circular geometry whereas two other configurations (needles with 24 and 36 unites) gave elongated pores. Based on the SEM micrographics we have concluded that during the puncture the adhesive side (the puncture was always taking place from this side) of the tape is first deformed by the needles (see Fig. SI4 from electronic supporting information) to finally tear the non-adhesive surface of the tape at the needle-sharp point exit.

The slope of the positive sigmoidal signal (for [TMA^+] = 40 µM) dependency plotted in function of the applied scan rate (v) was always one order of magnitude lower (10^{-8} $cm^2 \cdot s^{-1}$) as compared with the similar dependency plotted for negative peak current (10^{-7} $cm^2 \cdot s^{-1}$). This was observed for three independent membranes (see Figs. SI5, SI6 and SI7) and indicates that the TMA^+ transfer from the aqueous to the organic phase is mainly governed by the radial diffusion [47]. The presence of the linear diffusion is much more pronounced for the back transfer, this is from the organic phase to the aqueous phase, as deduced from the peak shaped signal of the negative current [48]. The estimated thickness of the hemispherical diffusion (δ – hemisphere radius) zone on the aqueous phase side was calculated using Eq. (1) derived for the spherical microelectrode (based on our further deliberations we have assumed that the organic phase is located below the pore in the aqueous phase and takes the shape of a sphere/hemisphere) [49]:

$$\delta = \left(\frac{1}{\sqrt{\pi D t}} + \frac{1}{r}\right)^{-1} \quad (1)$$

where r is the hemispherical electrode radius taken to be 80 µm (estimation based on SEM micrography analysis) and t is the time calculated from the ITVs. Calculated δ values equal to around 72 µm for 3 mV·s^{-1} and around 61 µm for 30 mV·s^{-1}. In the employed configuration the spacing between pores (pore center-to-center distance, d) was always greater than the 1300 µm. As such, it is safe to assume that each ITIES formed below micro-punched pore behaves individually. Since d >> δ and >> r, the overlay between hemispherical diffusion (affected by a linear diffusion) zones of the neighboring pores, as indicated in the work by Davies and Compton [47], or Guo and Lindner [48], should not occur for the applied experimental conditions.

The exact position of the ITIES in respect to the pore edges is difficult to be predicted. Based on our estimates, we have found that the recorded ionic currents are one order of magnitude higher as compared with the ITIES that would form exactly within the pore at its edge (inlaid ITIES). As reported by Strutwolf et al. recess of the aqueous phase to the micropores used as the ITIES support leads to the drop in the study-state currents and eventual transition to the peak shaped response being a consequence of a pore walls shielding effect [50]. All these suggest the existence of (i) spherical pendant organic phase droplet leaking from the pore or (ii) organic phase film covering the pore and its surrounding. Since the dimensionality of formed pores exceeds the critical radius of the microelectrode (r > 25 µm), in either case, it is expected that the radial diffusion of the analyte to the ITIES from the aqueous phase side will be burden with a fraction of a linear diffusion. Due to the complexity of the system ITV based experiments do not allow differentiation between two indicated scenarios. To give an estimate of the electrochemical dimensionality of the ITIES formed within the single pore we have calculated the radius of the aperture (crude simplification assuming the circular shape of the pore is employed) formed in the membrane using Eqs. (2)–(4).

Equation describing limiting current at the array of inlaid disc electrodes [51]:

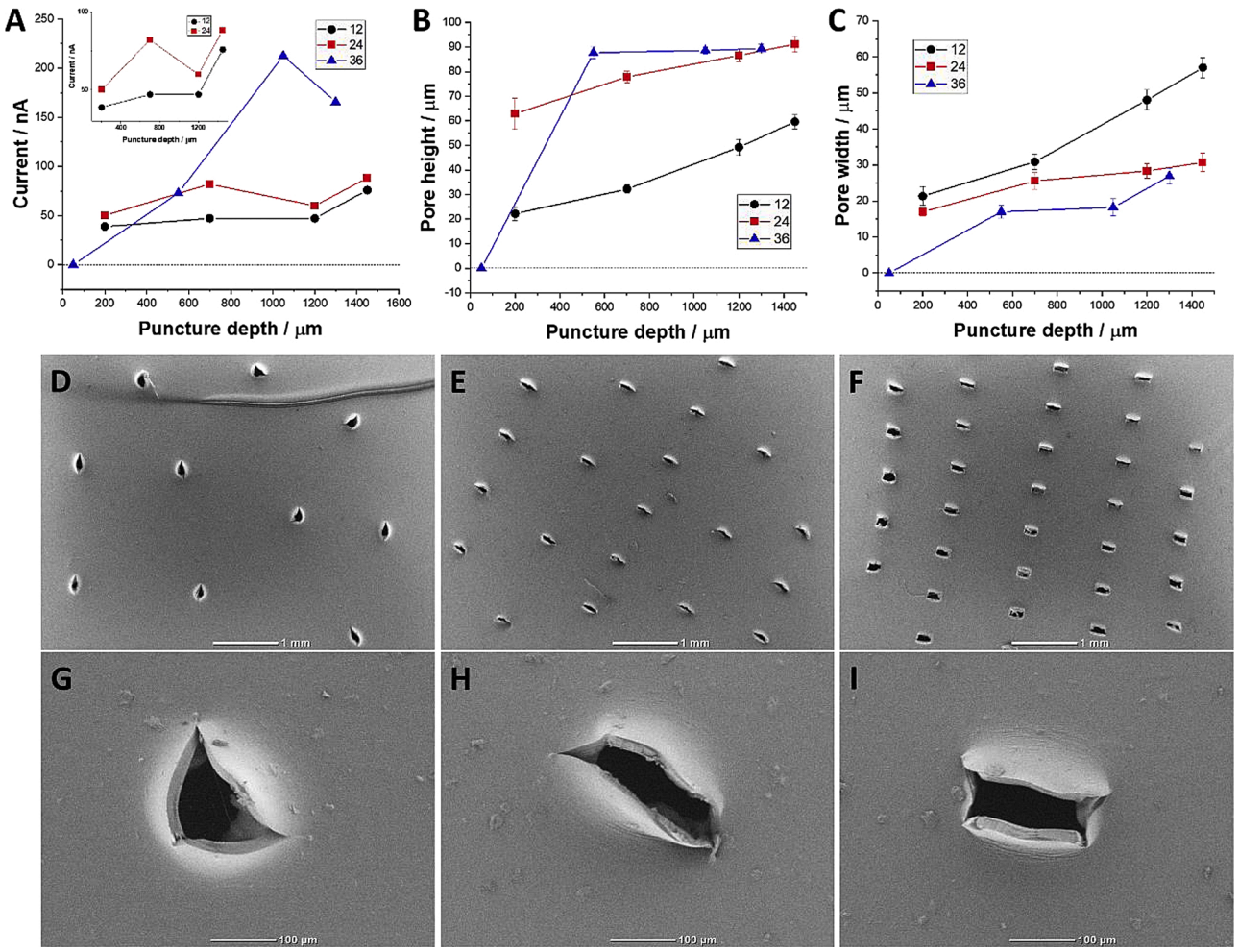

Fig. 3. A - Positive signal values for four studied penetration depths (see section 3.1 for details) and three different needle arrangements (12; 24 and 36 needles in an array). The number in the legend indicates the number of needles available within the array. ITVs were recorded at [TMA^+] = 40 μM. The scan rate was 25 $mV{\cdot}s^{-1}$. The dashed horizontal line indicates the zero current case – membrane was not punctured. Inset are the data points for the membranes with 12 or 24 openings. B - dependence of the pore height (longer section of the pore) vs the puncture depth (dimensions are based on photos taken with an optical microscope). C - dependence of the pore (shorter section of the pore) width vs the puncture depth (dimensions are based on photos taken with an optical microscope). Solid lines are only the guide to the eye. D, E, and F – SEM micrographics recorded at lower magnification for membranes with 12; 24, and 36 micro-openings, respectively. G, H, and I are the SEM micrographics of a single micro-pore from an array consisting of 12; 24, and 36 micro-openings, respectively. The membranes were prepared at penetration depth equal to 1450 μm (D, E, G and H) and 1300 μm (F and I).

$$I_{lim} = 4NzFDCr \quad (2)$$

Equation describing limiting current at the array of microelectrodes having a shape of hemisphere [52]:

$$I_{lim} = 2\pi NzFDCr \quad (3)$$

or sphere [52]:

$$I_{lim} = 4\pi NzFDCr \quad (4)$$

where N is the number of pores in the tape, z is the charge of the ion undergoing ion transfer reaction, F is the Faraday constant (96,458 C mol^{-1}), D is the diffusion coefficient (in $m^2{\cdot}s^{-1}$), C is the concentration (in mol m^{-3}), and r is the pore radius. Using the slopes of the calibration curves recorded for TMA^+ and ephedrine (I_{lim}/C, see Table 1 - sensitivity values) and the corresponding diffusion coefficients ($D_{TMA^+} = 13.8{\cdot}10^{-6}$ cm^2s^{-1} [53]; $D_{ephedrine} = 11.6{\cdot}10^{-6}$ cm^2s^{-1} [54]) we have estimated the values of a single pore radius for three different scenarios (Eqs. 2–4). The values being in line with the SEM micrographics analysis were obtained for the case where ITIES takes the spherical shape and are equal to around 50 ± 11 μm for TMA^+ and 37 ± 7 μm for ephedrine. Just for comparison, the radius calculated using Eq. (3) was equal to 102 ± 22 μm and 74 ± 13 μm, and using Eq. (2) was equal to 159 ± 34 μm and 116 ± 21 μm for TMA^+ and ephedrine, respectively. This rough simplifications indicate that the ITIES surface holds the same order of magnitude

Table 1
The summary of the electroanalytical parameters obtained for studied analytes (TMA^+, ephedrine alone, and ephedrine in the presence of the caffeine) at the ITIES supported with micro-punched membranes. Number of pores – 12. Penetration depth – 1450 μm. The error bars were calculated based on the values obtained for three independent experiments. For TMA^+ see Figs. SI8, SI9 and, SI10. For ephedrine see Figs. 5B, SI11 and, SI12.

Parameter	TMA^+	Ephedrine	Ephedrine in the presence of caffeine
Sensitivity (+) / AMm^{-1}	$1.02 \cdot 10^{-3} \pm 2.17 \cdot 10^{-4}$	$6.25 \cdot 10^{-4} \pm 1.07 \cdot 10^{-4}$	$4.61 \cdot 10^{-4}$
Sensitivity (-) / AMm^{-1}	$2.12 \cdot 10^{-3} \pm 2.57 \cdot 10^{-4}$	$7.28 \cdot 10^{-4} \pm 1.09 \cdot 10^{-4}$	$3.08 \cdot 10^{-4}$
LOD (+) / μM	$1.50 \cdot 10^{-6} \pm 7.82 \cdot 10^{-7}$	$4.07 \cdot 10^{-6} \pm 5.33 \cdot 10^{-7}$	$3.08 \cdot 10^{-6}$
LOD (-) / μM	$1.07 \cdot 10^{-6} \pm 3.04 \cdot 10^{-7}$	$3.82 \cdot 10^{-6} \pm 1.71 \cdot 10^{-6}$	$3.62 \cdot 10^{-6}$

as the pore dimensions observed at SEM micrographics.

Created platforms can be successfully applied (and due to the reasons described above are limited to) for electroanalytical applications. The preparation protocol applied for the LLI miniaturization is extremely fast and simple. Moreover, obtained platforms can be prepared in a reproducible and repeatable manner as shown in Fig. 4. In order to evaluate these two parameters, we have prepared a miniaturization protocol (also described in this work) that was given to four different persons. Each person was asked to micro-punched seven pieces of polyimide tape that were further fixed to a glass tube. Once ITIES was formed within the pores of the prepared membranes the ITVs in the presence of [TMA^+] = 40 μM were recorded and the limiting currents were extracted. A high repeatability factor (or the success rate) was obtained. Two persons successfully prepared (seven out of seven) fully functional platforms whereas for two other five out of seven or four out of seven membranes gave satisfactory results, respectively. As for the reproducibility, we compared the average forward peak currents vales which were found within the experimental error bars for all four tested sets. From the electroanalytical applications point of view, obtained discrepancies of the membrane to membrane electrochemical output imposes the necessity to individually check and calibrate all formed platforms. This is something we have to comprise for the cost of the system's simplicity.

3.2. Micropunched membranes application for sensing at ITIES

Based on the initial characterization of all micro-punctured membranes, we have chosen polyimide films patterned with the array of 12 needles with the penetration depth equal to 1450 μm. Not only this configuration gave membranes with the most circular pores, but also the center to the center distance between the neighboring pores was sufficiently high to prevent the overlap of the individual diffusion zones established below each pore. Figs. SI 8A–SI 10A shows the ITVs with corresponding calibration curves (Figs. SI 8B–SI 10B) recorded for TMA^+ in the range from 0.5 μM to 40 μM. During the interfacial polarization from lower to higher (the forward scan) and then from higher to lower (on the reversed scan) potential differences values, we have observed gradually increasing positive and negative signals attributed to the TMA^+ interfacial ion transfer, respectively. The sensitivity of the obtained calibration curves ($1.0{\cdot}10^{-3}$ $A{\cdot}M^{-1}$) are two orders of magnitude higher as the detection sensitivity obtained for the same model ion studied at the single pore microcapillary ($1.2{\cdot}10^{-5}$ $A{\cdot}M^{-1}$) [31,33]. Interestingly, the slope of the calibration curve for the reversed signal is twice bigger as compared with the slope of the forward signal being in line with our previous reports [31,33] and what was reported by others [55]. Presumably, this difference can be attributed to the partial pre-concentration of the analyte within the pore of the membrane or the thin film of the organic phase formed at the membrane surface. The lower limit of detection for the proposed configuration was calculated with the following equation:

$$LOD = \frac{3.3SD}{S} \quad (5)$$

where SD and S are the standard deviations of intercept and the slope of the calibration curve, respectively (these values were taken from the linear fit equation parameters). Calculated lower LOD values for positive and negative signal currents are equal to 1.5 μM and 1.1 μM, respectively. These values are within the expected order of magnitude for miniaturized ITIES and are even slightly higher than the concentration (0.5 μM) for which we started observing signals originating from the TMA^+ crossing the interface [53].

We have used the electrified LLI supported with the micro-punched membrane to electroanalytical evaluate the interfacial behavior of ephedrine. Fig. 5 shows the ITVs for the increasing concentration of ephedrine (from 1 μM to 70 μM) always initially present in the aqueous phase. Again, in agreement with what we have described above, the positive current related to the ephedrine transfer from the aqueous to the organic phase gives sigmodal current pattern partly overlaid with the limiting current (Na^+ transfer from the aqueous to the organic phase) characteristic for the analyte which mass transfer is (in that case mainly) governed by hemispherical diffusion. On the back transfer which is happening partially inside the pore, and hence, is limited by the linear diffusion, a negative peak was recorded. We have found that the corresponding calibration curve (see Fig. 5B) is linear in the entire studied concentration range. The ephedrine detection sensitivity calculated based on three independent repetitions was equal to $6.25 \cdot 10^{-4} \pm 1.07 \cdot 10^{-4}$ $A{\cdot}M^{-1}$ (see Figs. 5 and SI 11 and 12). The lower LODs calculated using Eq. (5) were equal to 4.1 μM for the positive and 3.8 μM for the negative signals, respectively.

Ephedrine used as the weight loss agent is frequently formulated with caffeine which is increasing its pharmacological effect. Caffeine is also considered as the main cutting agent of methamphetamine and amphetamine street samples which are structural analogs of ephedrine, and hence, are expected to give similar electroanalytical characteristics at the electrified LLI. These are the main reasons why we decided to investigate the potential interference of caffeine on ephedrine electroanalytical detection. Fig. 6 shows two sets of experiments performed to assess the interfacial behavior of ephedrine in the presence of caffeine always initially present in the aqueous phase. At given pH (~6), both species will be protonated ($pK_{a\ ephedrine} = 9.6$ [56] ; $pK_{a\ caffeine} = 10.4$ [57]) and may cross the electrified LLI when proper Galvani potential difference is applied [19,58]. The ITVs from Fig. 6A were recorded for the fixed concentration of ephedrine equal to 100 μM and increasing concentration of caffeine from 50 to 500 μM. The resulting faradaic currents were plotted and are shown in Fig. 6B. We found that for the studied caffeine concentration range, the forward peak current related to ephedrine transfer from the aqueous to the organic phase was practically unaffected (the % change did not exceed 7 %). Also, when only caffeine was present in the aqueous phase no change in the recorded currents for the positive side of the potential window were recorded – see Fig. SI13. The ITVs from Fig. 6C (and corresponding calibration curves from Fig. 6D) shows the effect of increasing ephedrine concentration in the cell containing 1 mM caffeine. Again, the calibration curve

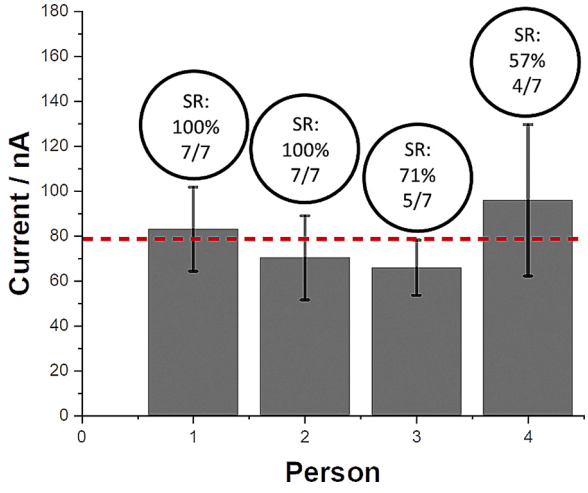

Fig. 4. Reproducibility and repeatability test for four independent sets of membranes (7 membranes were prepared for each set) tested by four different persons. The numbers in the circles indicate the success rate (SR). ITV was used for each membrane characterization. Following experimental conditions were applied and fixed for every test: [TMA^+] = 40 μM; scan rate = 25 $mV{\cdot}s^{-1}$; membranes with 12 micropores made with the protrusion of the needle equal to 1450 μm were used. The red dashed vertical line is the average current equal to 79 nA. (For interpretation of the references to colour in this figure legend, the reader is referred to the web version of this article).

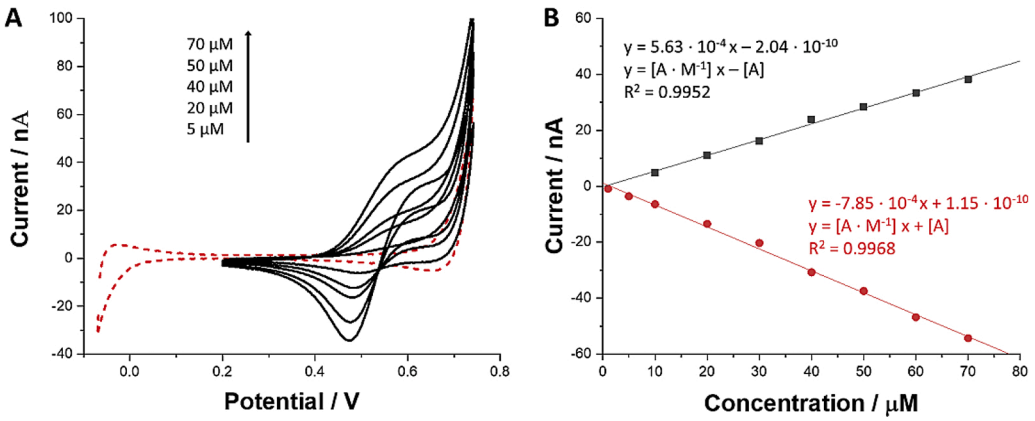

Fig. 5. A – ITVs recorded for the increasing concentration of ephedrine (red dash line is a blank) initially dissolved in the aqueous phase. The scan rate was 25 $mV{\cdot}s^{-1}$. The tested concentration of ephedrine was in the range from 1 µM to 70 µM. A membrane with 12 micropores prepared with penetration depth equal to 1450 µm was used as the ITIES support. B – positive and negative current intensities plotted in function of the increasing ephedrine concentration in the aqueous phase. Linear fitting parameters for the positive and negative currents are given in the upper and bottom section of the figure, respectively. pH of the aqueous phase was equal to around 6. (For interpretation of the references to colour in this figure legend, the reader is referred to the web version of this article).

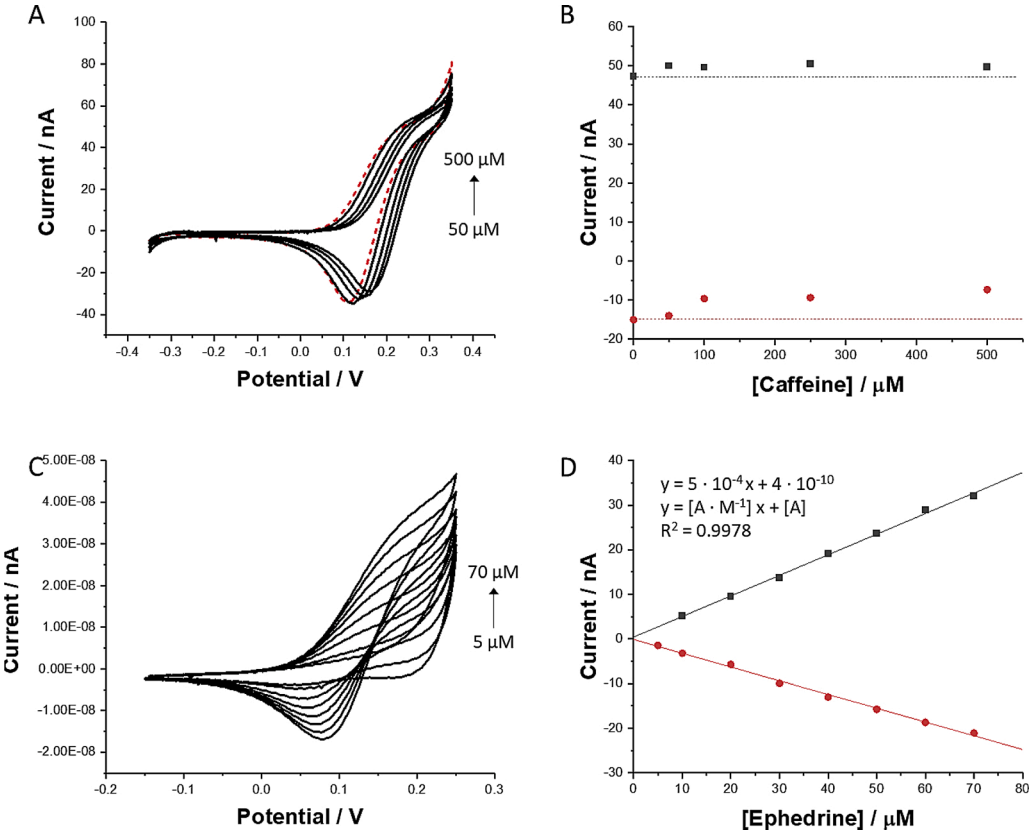

Fig. 6. A – ITVs recorded for the increasing concentration of caffeine (from 50 µM to 500 µM) and a fixed concentration of [ephedrine] = 100 µM (red dash line is a CV recorded in the absence of caffeine) initially dissolved in the aqueous phase. B – positive and negativecurrent intensities originating from the [ephedrine] = 100 µM interfacial ion transfer plotted in function of the increasing concentration of caffeine (prepared based on section A); C – ITVs recorded for the increasing concentration of ephedrine (from 5 µM to 70 µM) in the presence of fixed [caffeine] =1 mM. D – positive and negative current intensities plotted in function of the increasing ephedrine concentration in the presence of fixed [caffeine] =1 mM (prepared based on section C). In each case, the scan rate was equal to 25 $mV{\cdot}s^{-1}$. Ephedrine and caffeine were always initially present in the aqueous phase. (For interpretation of the references to colour in this figure legend, the reader is referred to the web version of this article).

was linear in the entire studied ephedrine concentration range. The resulting detection sensitivity equal to 0.3 – $0.5{\cdot}10^{-3}$ $A{\cdot}M^{-1}$ is very similar to the sensitivity values recorded in the absence of caffeine. Based on these observations we can conclude that caffeine has no (or very little) effect on the detection of ephedrine at polarized LLI which further underlines the practical utility of the developed method. To further support our conclusions, in Table 1 we have summarized the electroanalytical parameters obtained at miniaturized ITIES for TMA^+, ephedrine alone, and ephedrine in the presence of caffeine. As a matter of fact, the resultant of a few $logP_{o/w}$ predications for amphetamine (1.91) and methamphetamine (2.25) suggests that these molecules hold slightly lower affinity to the aqueous phase as compared with ephedrine (0.97), and hence, should undergo interfacial ion transfer at less positive potential values. This indicates that the developed platform can be further extended to other relevant analytes. We are currently working on this topic.

4. Conclusions

In this work, we have developed a fast and cheap protocol allowing for the preparation of patterned membranes that were used as a support of the electrified liquid-liquid interface. In this respect, we employed a self-adhesive polyimide tape that was punctured with three sets of prearranged needles. The effect of a number of pores and the puncture

depth on the electrochemical performance was studied and described. Based on the voltammetric and microscopy characterization we concluded that liquid-liquid interface leaks from the pore forming either array of pendant droplets or organic film covering the pore and its surrounding. In any case, our protocol provided repeatable and reproducible devices that were employed for ephedrine sensing alone and in the presence of its relevant and potential chemical interference – caffeine. Our method allows for the ephedrine detection with a lower LOD equal to around 4 μM. It is important to indicate that constructed platform are intended for sensing. More demanding applications employing electrified and miniaturized LLIs require further improvement.

CRediT authorship contribution statement

Paulina Borgul: Validation, Formal analysis, Investigation, Data curation, Writing - original draft, Visualization. **Patrycja Pawlak:** Validation. **Konrad Rudnicki:** Validation, Writing - review & editing. **Karolina Sipa:** Validation, Investigation, Writing - review & editing. **Pawel Krzyczmonik:** Resources. **Anna Trynda:** Resources, Writing - review & editing. **Slawomira Skrzypek:** Supervision, Writing - review & editing. **Grégoire Herzog:** Writing - review & editing. **Lukasz Poltorak:** Conceptualization, Methodology, Validation, Writing - original draft, Writing - review & editing, Visualization, Supervision, Funding acquisition.

Declaration of Competing Interest

The authors report no declarations of interest.

Acknowledgments

This project was financially supported by the National Science Center (NCN) in Krakow, Poland (Grant no. UMO-2018/31/D/ST4/03259).

Appendix A. Supplementary data

Supplementary material related to this article can be found, in the online version, at doi:https://doi.org/10.1016/j.snb.2021.130286.

References

[1] J. Koryta, Electrochemical polarization phenomena at the interface of two immiscible electrolyte solutions, Electrochim. Acta 24 (1979) 293–300, https://doi.org/10.1016/0013-4686(79)85048-3.
[2] G.C. Gschwend, A. Olaya, P. Peljo, H.H. Girault, Structure and reactivity of the polarised liquid–liquid interface: what we know and what we do not, Curr. Opin. Electrochem. 19 (2020) 137–143, https://doi.org/10.1016/j.coelec.2019.12.002.
[3] G.C. Gschwend, H.H. Girault, Discrete Helmholtz model: a single layer of correlated counter-ions. Metal oxides and silica interfaces, ion-exchange and biological membranes, Chem. Sci. 11 (2020) 10304–10312, https://doi.org/10.1039/d0sc03748f.
[4] Z. Samec, Dynamic electrochemistry at the interface between two immiscible electrolytes, Electochim. Acta 84 (2012) 21–28, https://doi.org/10.1016/j.electacta.2012.03.118.
[5] L. Poltorak, A. Gamero-Quijano, G. Herzog, A. Walcarius, Decorating soft electrified interfaces: from molecular assemblies to nano-objects, Appl. Mater. Today 9 (2017) 533–550, https://doi.org/10.1016/j.apmt.2017.10.001.
[6] T.J. Stockmann, Z. Ding, Uranyl ion extraction with conventional PUREX/TRUEX ligands assessed by electroanalytical chemistry at micro liquid/liquid interfaces, Anal. Chem. 83 (2011) 7542–7549, https://doi.org/10.1021/ac2018684.
[7] M.N. Jajuli, M.H. Hussin, B. Saad, A.A. Rahim, M. Hébrant, G. Herzog, Electrochemically modulated liquid-liquid extraction for sample enrichment, Anal. Chem. 91 (2019) 7466–7473, https://doi.org/10.1021/acs.analchem.9b01674.
[8] R.A.W. Dryfe, Modifying the liquid/liquid interface: pores, particles and deposition, Phys. Chem. Chem. Phys. 8 (2006) 1869–1883, https://doi.org/10.1039/b518018j.
[9] M.C. Collins, M. Hébrant, G. Herzog, Ion transfer at polarised liquid-liquid interfaces modified with adsorbed silica nanoparticles, Electrochim. Acta 282 (2018) 155–162, https://doi.org/10.1016/j.electacta.2018.06.036.
[10] H.A. Santos, V. García-Morales, C.M. Pereira, Electrochemical properties of phospholipid monolayers at liquid-liquid interfaces, ChemPhysChem 11 (2010) 28–41, https://doi.org/10.1002/cphc.200900609.
[11] S. Amemiya, X. Yang, T.L. Wazenegger, Voltammetry of the phase transfer of polypeptide protamines across polarized liquid/liquid interfaces, J. Am. Chem. Soc. 125 (2003) 11832–11833, https://doi.org/10.1021/ja036572b.
[12] J.M. Olmos, C.M. Pereira, Electrochemical sensing and characterization of denatonium ion by ion transfer at polarized liquid/liquid interfaces, J. Electroanal. Chem. 859 (2020) 113860, https://doi.org/10.1016/j.jelechem.2020.113860.
[13] R. Gulaboski, V. Mirceski, S. Komorsky-Lovric, M. Lovric, Three-phase electrodes: simple and efficient tool for analysis of ion transfer processes across liquid-liquid interface—twenty years on, J. Solid State Electrochem. 24 (2020) 2575–2583, https://doi.org/10.1007/s10008-020-04629-8.
[14] S. Liu, Q. Li, Y. Shao, Electrochemistry at micro- and nanoscopic liquid/liquid interfaces, Chem. Soc. Rev. 40 (2011) 2236–2253, https://doi.org/10.1039/c0cs00168f.
[15] M. Arooj, D.W.M. Arrigan, R.L. Mancera, Characterization of protein-facilitated ion-transfer mechanism at a polarized aqueous/organic interface, J. Phys. Chem. B 123 (2019) 7436–7444, https://doi.org/10.1021/acs.jpcb.9b04746.
[16] S.-X. Guo, P.R. Unwin, A.L. Whitworth, Z. Jie, Microelectrochemical Techniques for Probing Kinetics at Liquid-Liquid Interfaces, 2004.
[17] F.O. Laforge, J. Carpino, S.A. Rotenberg, M.V. Mirkin, Electrochemical attosyringe, Proc. Natl. Acad. Sci. U.S.A. 104 (2007) 11895–11900, https://doi.org/10.1073/pnas.0705102104.
[18] S.E.C. Dale, P.R. Unwin, Polarised liquid/liquid micro-interfaces move during charge transfer, Electrochem. Commun. 10 (2008) 723–726, https://doi.org/10.1016/j.elecom.2008.02.023.
[19] L. Poltorak, I. Eggink, M. Hoitink, E.J.R. Sudholter, M. De Puit, Electrified soft interface as a selective sensor for cocaine detection in street samples, Anal. Chem. 90 (2018) 7428–7433, https://doi.org/10.1021/acs.analchem.8b00916.
[20] A. Mälkiä, P. Liljeroth, A.K. Kontturi, K. Kontturi, Electrochemistry at liquid monolayer-modified liquid-liquid interfaces as an improvement to drug partitioning studies, J. Phys. Chem. B 105 (2001) 10884–10892, https://doi.org/10.1021/jp011835e.
[21] P. Vazquez, G. Herzog, C. O'Mahony, J. O'Brien, J. Scully, A. Blake, C. O'Mathuna, P. Galvin, Microscopic gel-liquid interfaces supported by hollow microneedle array for voltammetric drug detection, Sens. Actuators B Chem. 201 (2014) 572–578, https://doi.org/10.1016/j.snb.2014.04.080.
[22] B. Huang, B. Yu, P. Li, M. Jiang, Y. Bi, S. Wu, Vitamin B1 ion-selective microelectrode based on a liquid-liquid interface at the tip of a micropipette, Anal. Chim. Acta 312 (1995) 329–335.
[23] M.M. Hossain, C.S. Kim, H.J. Cha, H.J. Lee, Amperometric detection of parathion and methyl parathion with a microhole-ITIES, Electroanalysis 23 (2011) 2049–2056, https://doi.org/10.1002/elan.201100190.
[24] C.J. Collins, C. Lyons, J. Strutwolf, D.W.M. Arrigan, Serum-protein effects on the detection of the β-blocker propranolol by ion-transfer voltammetry at a micro-ITIES array, Talanta 80 (2010) 1993–1998, https://doi.org/10.1016/j.talanta.2009.10.060.
[25] S. Amemiya, Y. Kim, R. Ishimatsu, B. Kabagambe, Electrochemical heparin sensing at liquid/liquid interfaces and polymeric membranes, Anal. Bioanal. Chem. 399 (2011) 571–579, https://doi.org/10.1007/s00216-010-4056-2.
[26] E.D. Burgoyne, A.F. Molina-Osorio, R. Moshrefi, R. Shanahan, G.P. McGlacken, T. J. Stockmann, M.D. Scanlon, Detection of Pseudomonas aeruginosa quorum sensing molecules at an electrified liquid|liquid micro-interface through facilitated proton transfer, Analyst 145 (2020) 7000–7008, https://doi.org/10.1039/d0an01245a.
[27] B.N. Viada, L.M. Yudi, D.W.M. Arrigan, Detection of perfluorooctane sulfonate by ion-transfer stripping voltammetry at an array of microinterfaces between two immiscible electrolyte solutions, Analyst 145 (2020) 5776–5786, https://doi.org/10.1039/d0an00884b.
[28] G. Taylor, H.H. Girault, Ion transfer reactions across a liquid - liquid interface supported on a micropipette tip, J. Electroanal. Chem. 208 (1986) 179–183.
[29] J.A. Campbell, H.H. Girault, Steady state current for ion transfer reactions at a micro liquid/liquid interface, J. Electroanal. Chem. 266 (1989) 465–469, https://doi.org/10.1016/0022-0728(89)85091-0.
[30] V.J. Cunnane, D.J. Schiffrin, D.E. Williams, Micro-cavity electrode: a new type of liquid-liquid microelectrode, Electrochim. Acta 40 (1995) 2943–2946.
[31] K. Rudnicki, L. Poltorak, S. Skrzypek, E.J.R. Sudhölter, Fused silica micro-capillaries used for a simple miniaturization of the electrified liquid – liquid interface, Anal. Chem. 90 (2018) 7112–7116, https://doi.org/10.1021/acs.analchem.8b01351.
[32] S.N. Faisal, C.M. Pereira, S. Rho, H.J. Lee, Amperometric proton selective sensors utilizing ion transfer reactions across a microhole liquid/gel interface, Phys. Chem. Chem. Phys. 12 (2010) 15184–15189, https://doi.org/10.1039/c0cp00750a.
[33] K. Rudnicki, L. Poltorak, S. Skrzypek, E.J.R. Sudholter, Ion transfer voltammetry for analytical screening of fluoroquinolone antibiotics at the water – 1.2-dichloroethane interface, Anal. Chim. Acta 1085 (2019) 75–84, https://doi.org/10.1016/j.aca.2019.07.065.
[34] Y. Liu, A. Holzinger, P. Knittel, L. Poltorak, A. Gamero-Quijano, W.D.A. Rickard, A. Walcarius, G. Herzog, C. Kranz, D.W.M. Arrigan, Visualization of diffusion within nanoarrays, Anal. Chem. 88 (2016) 6689–6695, https://doi.org/10.1021/acs.analchem.6b00513.
[35] M.D. Scanlon, J. Strutwolf, A. Blake, D. Iacopino, A.J. Quinn, D.W.M. Arrigan, Ion-transfer electrochemistry at arrays of nanointerfaces between immiscible electrolyte solutions confined within silicon nitride nanopore membranes, Anal. Chem. 82 (2010) 6115–6123, https://doi.org/10.1021/ac1008282.

[36] N.T. Iwai, M. Kramaric, D. Crabbe, Y. Wei, R. Chen, M. Shen, GABA detection with Nano-ITIES pipet electrode: a new mechanism, water/DCE–octanoic acid interface, Anal. Chem. 90 (2018), https://doi.org/10.1021/acs.analchem.7b03099 acs.analchem.7b03099.
[37] S. Armaković, S. Armaković, Computational studies of stability, reactivity and degradation properties of ephedrine; a stimulant and precursor of illicit drugs, Adv. J. Chem. B. 2 (2020) 73–80.
[38] J.R. Docherty, Pharmacology of stimulants prohibited by the World Anti-Doping Agency (WADA), Br. J. Pharmacol. 154 (2008) 606–622, https://doi.org/10.1038/bjp.2008.124.
[39] N. Kurashima, Y. Makino, S. Sekita, Y. Urano, T. Nagano, Determination of origin of ephedrine used as precursor for illicit methamphetamine by carbon and nitrogen stable isotope ratio analysis, Anal. Chem. 76 (2004) 4233–4236, https://doi.org/10.1021/ac035417c.
[40] V.S. Vaidya, H.M. Mehendale, Ephedra. Encycl. Toxicol., third ed., 2014, pp. 426–430, https://doi.org/10.1016/B978-0-12-386454-3.00310-9.
[41] T.E. Graham, Caffeine, coffee and ephedrine: impact on exercise performance and metabolism, Can. J. Appl. Physiol. 26 (2001) 103–119, https://doi.org/10.1139/h2001-046.
[42] D. Molnár, K. Török, E. Erhardt, S. Jeges, Safety and efficacy of treatment with an ephedrine/caffeine mixture. The first double-blind placebo-controlled pilot study in adolescents, Int. J. Obes. Relat. Metab. Disord. 24 (2000) 1573–1578.
[43] A.G. Dulloo, Herbal simulation of ephedrine and caffeine in treatment of obesity, Int. J. Obes. 26 (2002) 590–592.
[44] Europol, Methamphetamine in Europe. EMCDDA-Europol Threat Assessment, 2019.
[45] T.J. Stockmann, A.-M. Montgomery, Z. Ding, Determination of alkali metal ion transfers at liquid|liquid interfaces stabilized by a micropipette, J. Electroanal. Chem. 684 (2012) 6–12, https://doi.org/10.1016/j.jelechem.2012.08.013.
[46] L. Xie, X. Huang, B. Su, Portable sensor for the detection of choline and its derivatives based on silica isoporous membrane and gellified nanointerfaces, ACS Sens. 2 (2017) 803–809, https://doi.org/10.1021/acssensors.7b00166.
[47] T.J. Davies, R.G. Compton, The cyclic and linear sweep voltammetry of regular and random arrays of microdisc electrodes: theory, J. Electroanal. Chem. 585 (2005) 63–82, https://doi.org/10.1016/j.jelechem.2005.07.022.
[48] J. Guo, E. Lindner, Cyclic voltammograms at coplanar and shallow recessed microdisk electrode arrays: guidelines for design and experiment, Anal. Chem. 81 (2009) 130–138.
[49] A. Molina, E. Laborda, J. Gonzalez, R.G. Compton, Effects of convergent diffusion and charge transfer kinetics on the diffusion layer thickness of spherical micro- and nanoelectrodes, PCCP 15 (2013) 7106–7113, https://doi.org/10.1039/c3cp50290b.
[50] J. Strutwolf, M.D. Scanlon, D.W.M. Arrigan, Electrochemical ion transfer across liquid/liquid interfaces confined within solid-state micropore arrays - simulations and experiments, Analyst 134 (2009) 148–158, https://doi.org/10.1039/b815256j.
[51] D.W.M. Arrigan, Nanoelectrodes, nanoelectrode arrays and their applications, Analyst 129 (2004) 1157–1165.
[52] R.M. Town, M. Tercier, N. Parthasarathy, F. Bujard, S. Rodak, C. Bernard, J. Buffle, A versatile macro- to micro-size stationary mercury drop electrode, Anal. Chim. Acta 302 (1995) 1–8, https://doi.org/10.1016/0003-2670(94)00442-O.
[53] L. Poltorak, K. Morakchi, G. Herzog, A. Walcarius, Electrochemical characterization of liquid-liquid micro-interfaces modified with mesoporous silica, Electrochim. Acta 179 (2015) 9–15, https://doi.org/10.1016/j.electacta.2015.01.129.
[54] A.J.M. Valente, A.C.F. Ribeiro, J.M.C. Marques, P.E. Abreu, V.M.M. Lobo, R. Kataky, Transport properties of aqueous solutions of (1R,2S)-(-)- and (1S,2R)-(+)-ephedrine hydrochloride at different temperatures, J. Chem. Eng. Data 55 (2010) 1145–1152, 2010.
[55] E. Alvarez De Eulate, J. Strutwolf, Y. Liu, K. O'Donnell, D.W.M. Arrigan, An electrochemical sensing platform based on liquid-liquid microinterface arrays formed in laser-ablated glass membranes, Anal. Chem. 88 (2016) 2596–2604, https://doi.org/10.1021/acs.analchem.5b03091.
[56] J.K. Lokhnauth, N.H. Snow, Solid phase micro-extraction coupled with ion mobility spectrometry for the analysis of ephedrine in urine, J. Sep. Sci. 28 (2005) 612–618, https://doi.org/10.1002/jssc.200401924.
[57] A. Karnjanapiboonwong, A.N. Morse, J.D. Maul, T.A. Anderson, Sorption of estrogens, triclosan, and caffeine in a sandy loam and a silt loam soil, J. Soils Sediments 10 (2010) 1300–1307, https://doi.org/10.1007/s11368-010-0223-5.
[58] L. Poltorak, K. Rudnicki, V. Kolivoška, T. Sebechlebská, P. Krzyczmonik, S. Skrzypek, Electrochemical study of ephedrine at the polarized liquid-liquid interface supported with a 3D printed cell, J. Hazard. Mater. 402 (2021) 123411, https://doi.org/10.1016/j.jhazmat.2020.123411.

Paulina Brogul received her MSc in Chemistry from University of Lodz in 2018. She is currently on her 3rd year of Ph.D. studies at the same university. Her research activities are related to the development of new fabrication technologies for the electrified liquid-liquid interface miniaturization and its further application to illicit drugs sensing.

Patrycja Pawlak is a BSc student studding at the Faculty of Chemistry, University of Lodz. She is currently an intern working under dr. Lukasz Poltorak supervision.

Konrad Rudnicki is an assistant professor at the Department of Inorganic and Analytical Chemistry at the University of Lodz. He obtained his Ph.D. in 2019. He is a member of the Polish Chemical Society (PTChem) and The International Society of Electrochemistry (ISE). His research is focused on analysis of biologically active compounds, such as pesticides, drugs and antibiotics using electrochemical methods – cyclic voltammetry (CV), square wave voltammetry (SWV) and ion transfer voltammetry (ITV). He is also strongly interested in fabrication of new type of microdevices based on the electrified liquid – liquid interface and modification of solid electrodes.

Karolina Sipa obtained a doctoral degree in chemistry from the University of Lodz (Poland) in 2019 where she is currently hired as the assistant professor. She is a member of Polish Chemical Society and International Society of Electrochemistry. Her main scientific interests cover the trace analytical chemistry, electroanalysis, conductive surface modification and characterization, development of smart and functional materials for sensing applications.

Paweł Krzyczmonik studied Chemistry at the University of Łódź, Poland, and received his doctoral degree in Chemistry in 1991. He was a scholarship holder at the University of Szeged, Hungary and the Ecole Nationale Supérieure de Chimie de Montpellier, France. He works in the Team of Electroanalysis and Electrochemistry in the Department of Inorganic and Analytic Chemistry, Faculty of Chemistry, University of Łódź, Poland. His current research interests are conductive polymers, modified electrodes, electroanalysis and electrochemical biosensors, systems with immobilized, enzymes electroanalysis of bioactive substances. He is a member of ISE.

Anna Trydna Anna Trydna received her Ph.D. from University of Gdansk, Faculty of Chemistry in chemical science through a distinguished thesis in 2001. From 2001–2008 she was a forensic chemistry expert in the Voivodeship Police Forensic Laboratory in Gdansk to become the Deputy Head of the Laboratory and Quality Manager in 2009. Dr. Trynda was responsible for, among others, the implementation of ISO/IEC 17025:2005 compliant quality system in the Gdańsk laboratory which resulted in obtaining the certificate from the Polish Centre for Accreditation. Since 2013 she is the head of Chemistry Department in Central Forensic Laboratory of the Police in Warsaw, Poland. Her main scientific areas are: chemical analysis of drugs, illegal drug laboratories including organic synthesis methods and implementation of new analytical methods in forensic chemistry.

Sławomira Skrzypek (D.Sc. Ph.D.) is an Associate Professor at the Department of Inorganic and Analytical Chemistry at the University of Lodz. She is a member of the Polish Chemical Society and International Society of Electrochemistry. Her research are focused on the electrochemical study and the determination of pesticides and other biological active compounds at solid electrodes, modification of electrode materials surfaces, determination of compounds with guanidine group as catalysts for hydrogen reduction.

Grégoire Herzog received his Ph.D. in Chemistry from University College Cork, Ireland in 2004. after a post-doc at the Université Joseph Fourier in Grenoble, France, he joined the Tyndall National Institute where he worked on the development of miniaturized electroanalytical tools based on ion transfer voltammetry at liquid–liquid interfaces. Since 2011, he is a researcher at the Laboratoire de ChimiePhysique et Microbiologie pour l'Environnement (CNRS – Université de Lorraine,France) where is reserach focuses on the modification of modified liquid-liquid interfaces.

Lukasz Poltorak received his Ph.D. from Lorraine University (Nancy, France) in Chemistry in 2015. From 2015 till 2018 he was working as the post-doctoral fellow at Delft University of Technology in Organic Materials & Interfaces group (The Netherlands). Since 2019 he is hired as the assistant professor working the Faculty of Chemistry, University of Lodz (Poland). His main scientific interest cover electrochemistry of soft interfaces, including electrified liquid-liquid interfaces, electrochemistry of membranes, (bio)sensors development, biointerfaces investigation and electrochemistry of soft matter.